

# Design and Fabrication of a Compact, Low-Cost UHF-RFID Repeater, Exploiting Circular Cross-Polarization

Spyros Megalou, Antonis G. Dimitriou *Senior Member, IEEE*, Anastasios Tzitzis, Traianos V. Yioultsis, *Member, IEEE*,

**Abstract**—In this paper we aim to increase the range of commercial passive UHF RFID technology. We propose a prototype forward-link repeater, which consists of a pair of antennas, a band pass filter, an RF power limiter and a low-noise amplifier (LNA). Initially, we focus on the design of the two antennas with inverse direction of circular polarization (CP), so that sufficient decoupling is ensured, while adhering to the following constraints: *i)* the input antenna is circularly polarized to maximize the gain towards the reader's antenna, *ii)* the output antenna is circularly polarized to improve the probability of successful tag reception, given the expected randomness in the tag's orientation, *iii)* the volume of the entire structure is kept small. Then, we present the achieved range improvement of the proposed repeater in two applications: *a)* a fixed installation, where the reader successfully identified passive RFID tags from 60m and *b)* by placing the repeater on top of an autonomous robot, to provide power in distant battery-less RFID tags, while the robot randomly moves inside a large area. The robotic-repeater prototype achieved remarkable performance, inventorying distant passive RFID tags, under Non-Line-Of-Sight (NLOS) conditions with the reader, exploiting the robot's mobility for fading-mitigation, combined with increased incident power from the repeater.

**Index Terms**—Radiofrequency identification, RFID tags, Decoupling Techniques, Repeater, Robot.

## I. INTRODUCTION

**R**ADIO Frequency Identification (RFID) technology is continuously growing its market share, replacing traditional barcode technology in logistics and representing the vessel for the establishment of new applications and empowering the Internet of Things. The evolution of the tag's front-end technology has allowed for improved sensitivity in the latest RFID ICs. As a result, passive RFID tags can be measured at twice the distance compared the technology ten years ago, achieving reliable read-ranges in the order of 6m. However, the infrastructure cost for larger areas remains an issue for the market penetration of the technology, since the cost for additional "reader+antennas" per unit area is still large.

Prior art concerning interrogation range improvement includes: *i)* configurations which are able to harvest energy

This work was supported by the European Union and Greek National Funds through the Operational Program Competitiveness, Entrepreneurship, and Innovation, under the call Research Create Innovate under Project TIEDK-03032. (Corresponding author: Antonis G. Dimitriou.)

The authors are with the School of Electrical and Computer Engineering, Aristotle University of Thessaloniki, 54124 Thessaloniki, Greece (e-mail: antodimi@ece.auth.gr).

Manuscript received 06/11/2020.

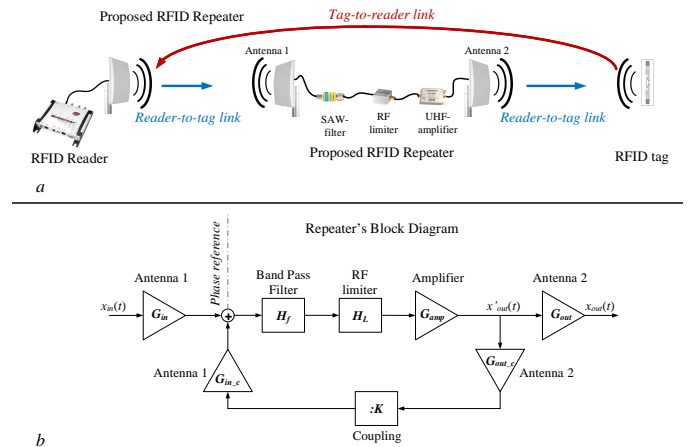


Fig. 1. Representation of the proposed repeater.

from harmonics [1]- [2], *ii)* configurations that use more than a single antenna and blind beamforming [3], *iii)* systems that power-optimize the conventional waveforms [4]- [5], *iv)* multistatic scatter radio technique [6]- [10] and even *v)* energy harvesting from other energy sources (i.e. solar energy) [11].

Recently a prototype, low-cost, forward-link repeater has been proposed, to increase the range of passive Radio Frequency Identification (RFID) systems [12]. The functionality and the corresponding block diagram are shown in Fig. 1. The proposed structure aims to amplify the RFID-reader transmitted UHF carrier signal; hence, it consists of *i)* a SAW-technology band-pass filter, to amplify only RFID in-band transmissions, *ii)* an RF-power-limiter to guarantee that neither the power that reaches the amplifier exceeds maximum allowable input, nor the output of the amplifier ever violates the maximum EIRP regulations, *iii)* a low noise, high-gain UHF amplifier and *iv)* a pair of antennas, facing opposite directions, functioning as input and output to the repeater. Experimental results with off-the-shelf equipment, presented in [12], demonstrated a measured range of 74m for passive RFID tags; a more than  $5\times$ -range improvement over the corresponding maximum measured range without the repeater.

Potential applications, discussed in [12], include placement of multiple repeaters in cascade to increase the "forward-link" illumination region of the reader in large areas, like parking-lots, exhibitions areas (the proposed structure will be installed in an exhibition area, identifying RFID-tagged visitors and

exhibits). Another application group is about illuminating a separate distant region (where a family of tags are placed) at larger distances (e.g. in harbors). The communication range could be further improved by exploiting the tag-to-reader link and result with a full duplex system. In a two-way repeater, there are two amplifiers, one for the reader-to-tag link and one for the tag-to-reader link. Isolation between the output and the input of each amplifier is necessary, otherwise the amplifiers would instantly saturate. Adaptive cancellation circuits would be necessary, increasing the cost and complexity of the proposed structure, as analysed in [12].

The most critical part in the design of the proposed structure is the antenna pair of Fig. 1. More specifically, the two antennas should comply to the following set of criteria:

- Both antennas should be circularly polarized. For the input antenna, this is to ensure maximum gain, since it is illuminated by a circularly polarized reader antenna and for the output antenna, to improve the probability of successful reception by the randomly oriented linearly polarized tag antenna.
- Decoupling between the output and the input antenna should be greater than the amplification (typically  $\geq 40\text{dB}$ ), otherwise, depending on the phase of the coupling, the amplifier might saturate.
- The volume of the structure should be kept small, despite the strict decoupling constraint: one should avoid placing the two antennas at greater distance or placing a "large" ground plane between the two antennas.

The challenge of isolation, is faced in a lot of applications that require proximity between antennas. In most cases, antennas are on the same plane or even printed on the same laminates (e.g. MIMO patch antennas). Prior art on isolation enhancement is focused on i) introducing coupling elements or resonators between antennas [13]-[15], ii) using decoupling networks [16]-[17], iii) alternating ground planes [18]-[20] and iv) utilizing metamaterial insulators [21]-[23]. In our case the two antennas of the repeater are on a different plane, facing opposite directions, as shown in Fig. 1. Despite the ground planes between the two antennas, the achieved decoupling did not meet the required level, to protect the amplifier from saturation. The aforementioned methods are not expected to provide a rigorous decoupling in this case, either due to the need of highly complicated structures and designs or due to the extremely close proximity of the two antennas, which does not provide the necessary space for additional inclusions.

In this paper, we propose the design of the two antennas with inverse handedness of circular polarization. A similar design was shortly presented in [24] where orthogonal polarization is exploited for repeater use from 1.53GHz to 1.603GHz. Taking advantage of this decoupling method we manufacture the prototype structure of such a repeater operating in the European UHF-RFID band (865-868MHz). By deploying the proposed technique, high isolation is achieved, regardless of the size of the structure. The input antenna should be oriented to the direction of the reader's antenna, to maximize input gain. The circularly cross-polarized field of the output antenna does not affect the backscattered field by the tags (that reaches the

reader's antenna), since the tag's antenna is linearly polarized.

The design of a single antenna is analyzed in Section II, based on theoretical models and simulations. The design of the entire structure is presented in Section III, including theoretical analysis and simulation results. Fabrication and measurements in an anechoic chamber are given in Section IV, achieving a decoupling of 60dB. The performance of the proposed repeater is investigated in Section IV.

Measurements performed outdoors verify the repeater's expected performance, successfully identifying commercial RFID tags from a commercial monostatic RFID reader at 60m. In addition we introduce a new application, where the repeater is placed on top of an autonomous moving robot (we have deployed the 600\$ turtlebot-2 robot). We show how a fixed reader with a single antenna, successfully identifies a distant large tag population inside a room, as the robot moves in the area. Thanks to the robot's mobility, passive RFID tags that are obstructed by several obstacles are successfully identified by the distant reader's antenna. A fleet of such robots could enhance the reading range of a fixed installation, while keeping the cost low, as discussed in Section V.

## II. SINGLE ANTENNA DESIGN

Initially, a circularly polarized microstrip antenna is designed. Design begins from theoretical models, then numerical simulations are carried out and prototypes are constructed and measured until specific goals with respect to bandwidth, gain and polarization are satisfied. Circular polarization is accomplished when two orthogonal patch modes are excited with  $90^\circ$  phase difference. Two types of feeding configurations can achieve CP [25]. The first type includes two feeding points where a 3dB divider is required and a  $\lambda/4$ -length feed line after the divider, to ensure the  $90^\circ$  delay. The second type is a single-point feed, where adjusting the feeding point position and physical shape of the patch is required.

The antenna of the repeater is a square single-fed circularly polarized patch antenna, as shown in Fig. 2. The design procedure[26], provides the calculation of the length  $L$  (equal to the width  $W$ ) of the patch.

Furthermore, as discussed in the introduction, circular polarization is an essential property in RFID reader-antenna design. As shown in Fig. 2, two opposite truncated corners are introduced in the patch geometry, which will generate the desired field, [27].

Having calculated the dimensions of the patch, one needs to define the feeding technique and the feed point. There are in general several antenna-feed-techniques, such as using a microstrip line, aperture coupling, a coaxial probe, or proximity coupling. The most appropriate method in this case is a coaxial probe, which is relatively easy to fabricate and has low spurious radiation compared with the microstrip line feed. Due to symmetry, the coaxial probe can be placed either on the  $x$  or the  $y$  axis. Depending on the locations of the truncated corners, with respect to the feed, right-hand (RH) or left-hand (LH) circular polarization can be selected, as will be shown in the following section. As a rule of thumb for the polarization handedness, one could define a vector, originating from the

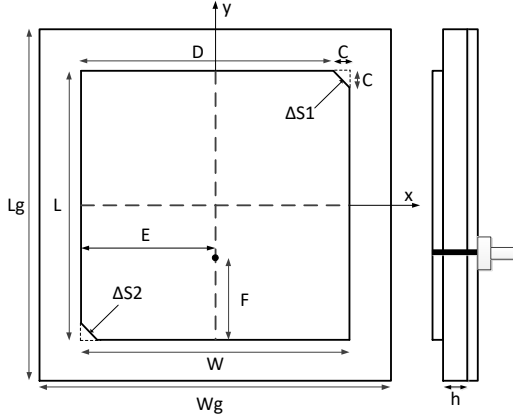


Fig. 2. Geometry of Proposed Antenna.

feed point to the center of the antenna (i.e. the cross-section of two axes in Fig. 2); if the nearest truncated corner from the feed point is located to the left of the vector, then we have a RHCP antenna, otherwise, LHCP is achieved.

The aforementioned theoretical analysis, represents a starting point for parametric simulations, in order to fine-tune the exact geometrical characteristics of the microstrip antenna, such that all design parameters are satisfied for the actual dielectric material; namely polarization, bandwidth and impedance matching. The optimization parameters are the length of the patch ( $L$ ), the length of the truncated corner ( $c$ ) and the feed point distance from the side of the patch ( $E$ ).

For the numerical analysis, a Finite Difference Time Domain (FDTD) method was applied. The proposed design is simulated and fabricated by using Rogers RT Duroid 5880 substrate with thickness  $h = 1.55$  mm and dielectric constant  $\epsilon_r = 2.2$ . Substrate and ground dimensions are  $200 \times 200 \text{mm}^2$ . The detailed results of the analysis are summarized in Table I, in accordance to the variables shown in Fig. 2. The feed location is set at the  $y$ -axis and as the nearest truncated corner is located to the left of it, RHCP is achieved. Best impedance matching and lowest axial ratio was obtained for a 36.8mm feed point distance from the bottom of the patch, a 59.2mm feed point distance from the side of patch and a truncated corner length  $c = 10$ mm. The reflection coefficient  $S_{11}$  is shown in Fig. 3, the achieved axial ratio in Fig. 4 and the far-field directivity pattern at 866MHz in Fig. 5. Both impedance-matching ( $S_{11} < -10$ dB) and circular polarization (Axial Ratio  $< 3$  dB) is achieved in the desired UHF-RFID European frequency band.

### III. BACK TO BACK ANTENNA DESIGN

Initially, the single antenna is duplicated and the two identical antennas are placed back-to-back, as desired in the configuration of the proposed repeater. The distance between the two antennas should be the smallest possible in order to achieve a compact design. The requirement of space for the connectors led to a 20mm back-to-back distance. The 3D design of the configuration of the two antennas is shown in Fig.

TABLE I  
DESIGN PARAMETERS

Initial parameters	
Width (W) (mm)	116.1
Length (L) (mm)	116.1
Feed distance from bottom of patch (F) (mm)	23.2
Feed distance from side of patch (E) (mm)	59.2
Side of truncated corner (C) (mm)	8
After simulations	
Width (W) (mm)	118.4
Length (L) (mm)	118.4
Feed distance from bottom of patch (F) (mm)	36.8
Feed distance from side of patch (E) (mm)	59.2
Side of truncated corner (c) (mm)	10

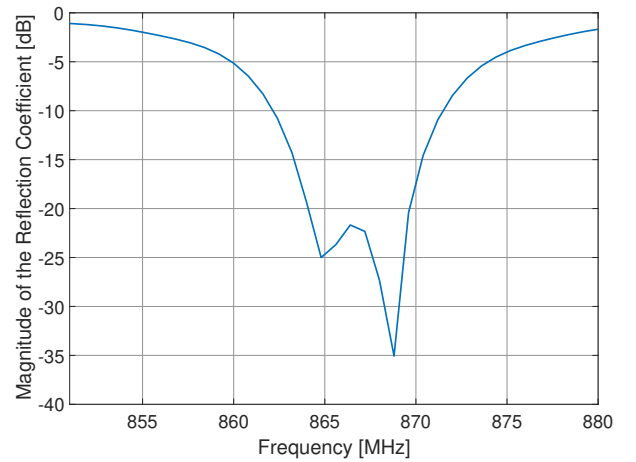


Fig. 3. Magnitude of the Reflection Coefficient of Single Antenna (dB).

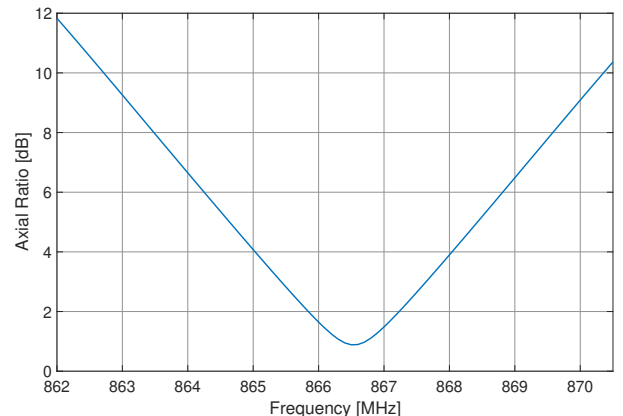


Fig. 4. Magnitude of Axial Ratio of Single Antenna (dB).

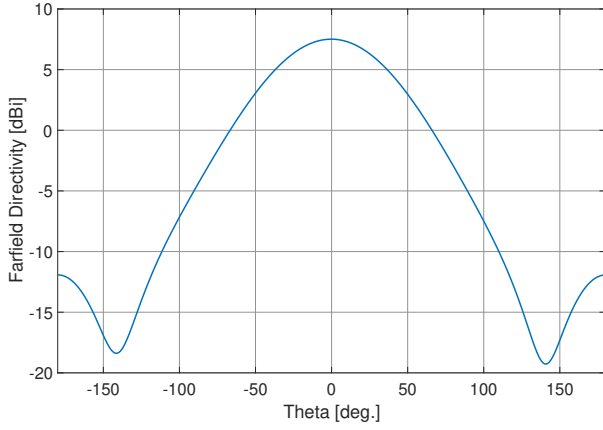


Fig. 5. Farfield Directivity Pattern of Single Antenna.

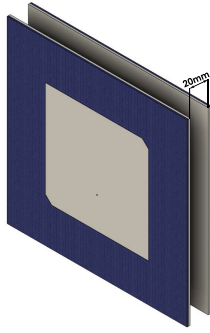


Fig. 6. Repeater Configuration with Two Identical Antennas.

6. In the following analysis, we are interested in the decoupling between the two antennas (which should be considerably larger than the repeater's gain). Moreover, the input impedance and polarization of each antenna should remain functional within the desired band, despite the close proximity of the two antennas. The simulated  $S_{21}$  between the two antenna ports, which describes the coupling among the two antennas, is shown in Fig. 7. The achieved decoupling of 34dB is clearly unacceptable in this case. In fact, an additional safety-margin in the design-phase should be introduced to make sure that the manufactured antenna pair is sufficiently decoupled.

#### A. Proposed Structure

Figure 8 shows a simplified block diagram of the repeater. The coupling here is represented by  $H_B(f)$  and the constraint can be written as:

$$H_B(f)G_{amp}(f) < 1 \text{ or } H_B(f) < \frac{1}{G_{amp}(f)} \quad (1)$$

The proposed solution in this case is to design the antennas of the repeater with different handedness of circular polarization; i.e. one antenna with RHCP and the other with LHCP. A simple representation of a circularly polarized antenna is illustrated in Fig. 9. Two generic antennas, shown as abstract dipoles or monopoles, are considered along the main polarization-excitation axes. A  $\lambda/4$ -length line feed is introduced between the  $x$ -axis and the  $y$ -axis and the feed

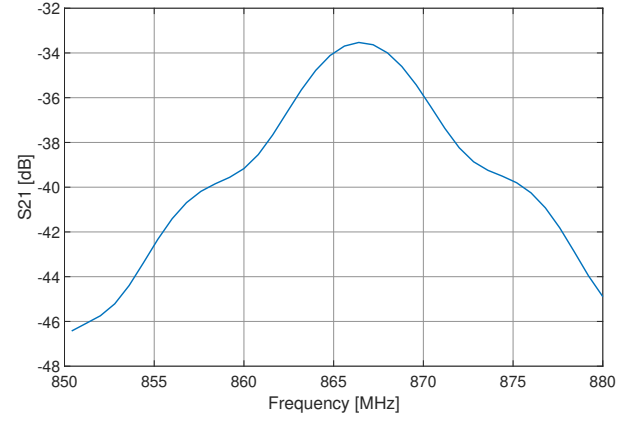
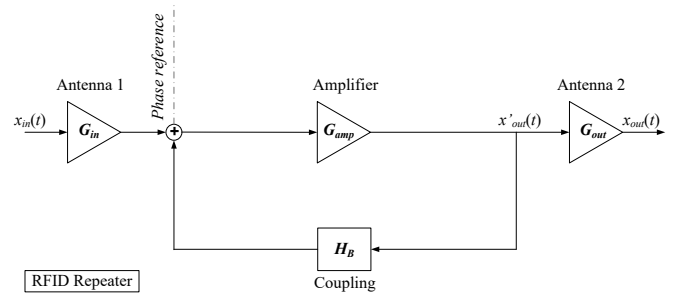

 Fig. 7.  $S_{21}$  parameter of repeater with two identical antennas.


Fig. 8. Simplified block diagram of the repeater.

is set at the  $+x$ -axis. When a current arrives at the feed point (exciting the  $x$ -polarized dipole), it will induce the same field along the  $y$ -polarized dipole with a  $T/4$  delay ( $T$  is the period of the wave), resulting in an equivalent phase-delay of  $90^\circ$ . This equivalent, shown in Fig. 9a creates a RHCP field. Similarly, if the current-feed is set at the  $+y$ -axis, the  $x$ -polarized field will be delayed by  $T/4$ . Considering the  $x$ -field as the time-reference, the phase-difference with the  $y$ -field will be  $+90^\circ$ , defined as LHCP. This is shown in Fig. 9b.

We now consider the direction of propagation of a RHCP wave along the  $+z$ -axis, as demonstrated in Fig. 10. The same RHCP antenna is placed opposite to the transmitting one. We note that the feed line is rotated, due to the two antennas placement, in order to face each other. The  $x$ -axis wave will arrive first and excite the  $-x$ -axis field of the receiver; i.e.  $E_{t_0=0} = -E_x$ . After  $T/4$  the  $y$ -axis field will arrive and excite

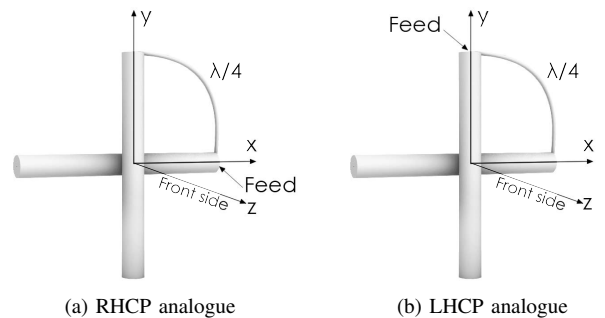


Fig. 9. Simple analogue of a RH and LH CP antenna.

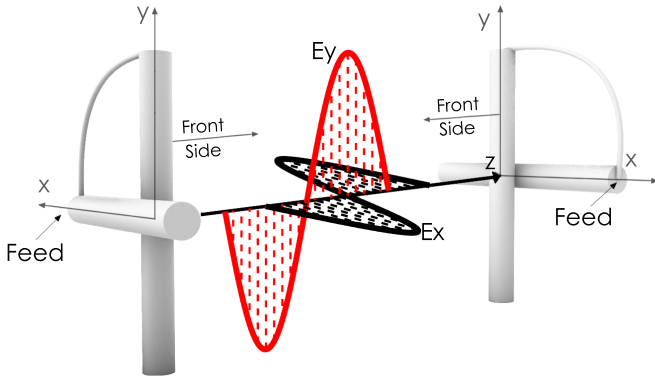


Fig. 10. Two antennas with the same polarization handedness facing each other.

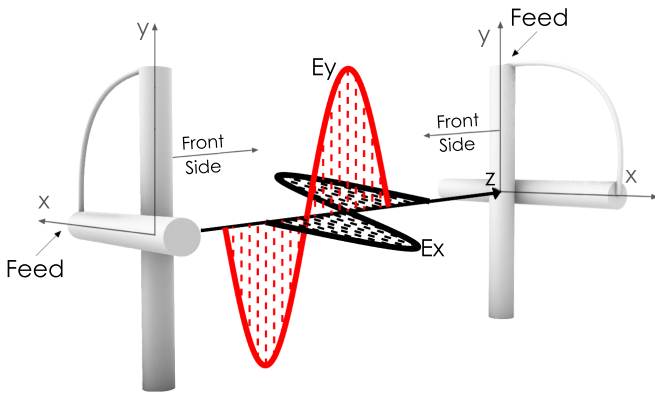


Fig. 11. Two antennas with opposite polarization handedness facing each other.

the  $+y$ -axis field of the receiver. Due to the  $\lambda/4$  delay line of the receiving antenna, the  $y$  field contributes to the total current that is summed to the current due to the  $x$  field after an additional  $T/4$  delay. Therefore, taking the incident  $E_x$  field as time reference, the total current at the receiver, will be given by:

$$I_{tot} \propto -E_x \cos(2\pi ft) + E_y \cos\left[2\pi f\left(t - \frac{T}{4} - \frac{T}{4}\right)\right] = - (E_x + E_y) \cos(2\pi ft) \quad (2)$$

Equation (2) states that when two CP antennas with the same direction of rotation face each other, the current at the receiver results from the constructive summation of the field from the polarization axes.

Following a similar analysis, consider the LHCP of Fig. 9b, opposite to the RHCP antenna, as shown in Fig. 11. Again, the  $x$ -axis field arrives first and excites the  $-x$ -axis field of the receiver; i.e.  $E_{t_0=0} = -E_x$ . Due to the  $\lambda/4$  delay line, it will reach the feed concurrently with the  $y$ -axis field. Therefore, the total current at the feed will be:

$$I_{tot} \propto -E_x \cos(2\pi ft) + E_y \cos(2\pi ft) = (E_y - E_x) \cos(2\pi ft) \quad (3)$$

Therefore, if  $E_y = E_x$ , the total current becomes zero.

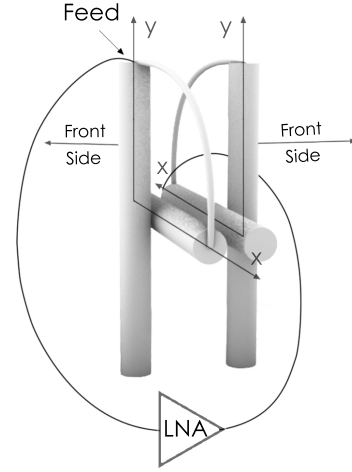


Fig. 12. Two CP antennas with inverse directions of polarization set in the configuration of the proposed repeater.

Exploiting this property for the repeater, we propose the design of two CP antennas with cross-polarized circular polarization, as shown in Fig. 12. The amplified current through the LNA excites the antenna to the right (the feed is at the  $x$ -axis), which is RHCP and represents the output of the repeater. An undesired field is coupled to the LHCP antenna to the left. The total current at the left antenna (input of the repeater) is:

$$I_{tot} \propto -E_x \cos\left[2\pi f\left(t - \frac{T}{4}\right)\right] + E_y \cos\left[2\pi f\left(t - \frac{T}{4}\right)\right] = (-E_x + E_y) \cos\left[2\pi f\left(t - \frac{T}{4}\right)\right] \quad (4)$$

Due to the vicinity of the two antennas, the magnitudes of  $E_y$ ,  $E_x$  are expected to be equal, since they are not affected by the environment and the totally undesired coupling becomes ideally zero, provided that the two antennas are circularly polarized. As the circular polarization becomes elliptical, away from the central frequency, the desired decoupling is expected to be somewhat reduced.

### B. Combined antenna design and simulations

As discussed on the previous section to achieve different polarization-direction, the location of the feeding point with respect to the position of the truncated corner needs to change. For the single antenna design in section II a RHCP antenna was designed by setting the feed at the  $y$ -axis and the nearest truncated corner is located on the left of it. In order to achieve LHCP a  $90^\circ$  rotation of the feeding point is needed as shown in Fig. 13.

Again, we simulated the new structure, considering the pair of antennas, placed at 20mm distance, in order to investigate the  $S_{21}$  performance. The results shown in Fig. 14 agree with the theoretical expectations, discussed earlier and verify that by using two antennas with different CP handedness decoupling has been increased to 62dB (achieving 28dB improvement over the results of Fig. 7). Furthermore, as the circular polarization becomes elliptical (Fig. 4), decoupling is reduced, as expected.

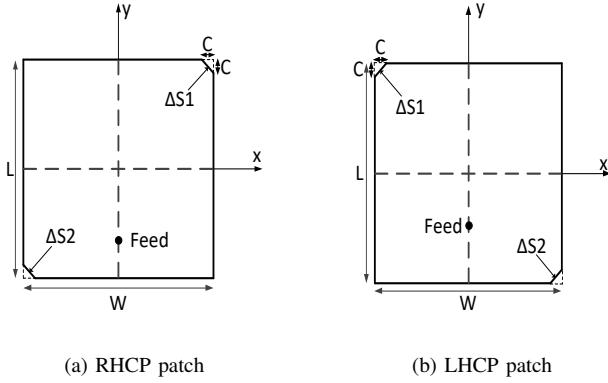


Fig. 13. Single feed right-hand and left-hand circularly polarized patch antenna.

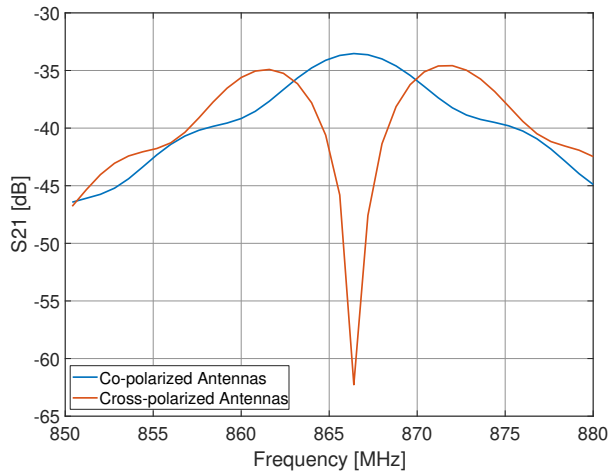


Fig. 14.  $S_{21}$  parameter simulation results for a repeater with two co- and cross-polarized CP antennas.

IV. FABRICATION AND MEASUREMENTS

Both antennas of the repeater are fabricated by the photo-lithographic method [28], using RT/duroid 5880 Laminates and the result is shown in Fig. 15.

All the measurements took place in an anechoic chamber, in order to minimize any electromagnetic interference and unwanted reflections. Three antennas were fabricated (two with RHCP and one with LHCP), in order to validate the performance of our proposed solution; i.e. compare the decoupling between two co-polarized CP antennas and two cross-polarized ones.

The measured reflection coefficient for all three antennas is shown in Fig. 16. Good impedance matching was measured for all antennas between 865 and 869 MHz. In Fig. 17 the measured directivity pattern vs the one derived from FDTD analysis is presented.

A non-conductive plastic casing was designed and fabricated using a 3D printer. The casing is responsible for holding the antennas at a fixed distance, facing opposite directions as shown in Fig. 18. The set-up was placed in the anechoic chamber and  $S_{21}$  was measured. Initially, decoupling ( $S_{21}$ ) between two antennas with RHCP was measured and then the corresponding decoupling between the proposed two antennas



Fig. 15. Single RHCP antenna fabricated by the photo-lithographic method.

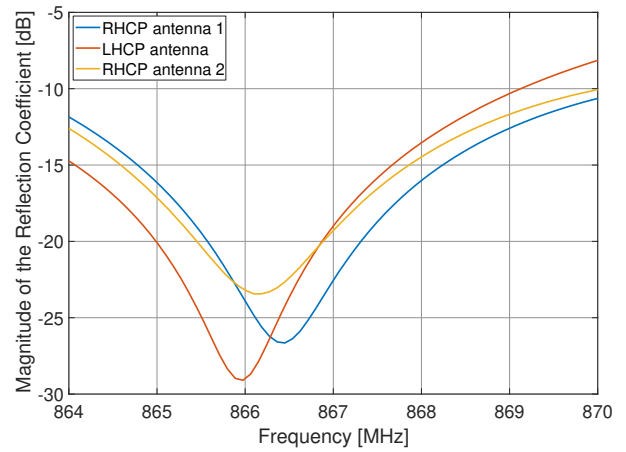


Fig. 16. Measured Magnitude of the Reflection Coefficient of the Three Antennas (dB).

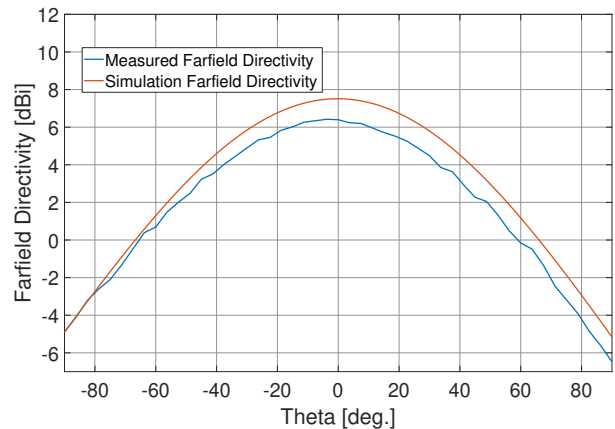


Fig. 17. Measured vs Simulated Farfield Directivity Pattern of Single RHCP Antenna

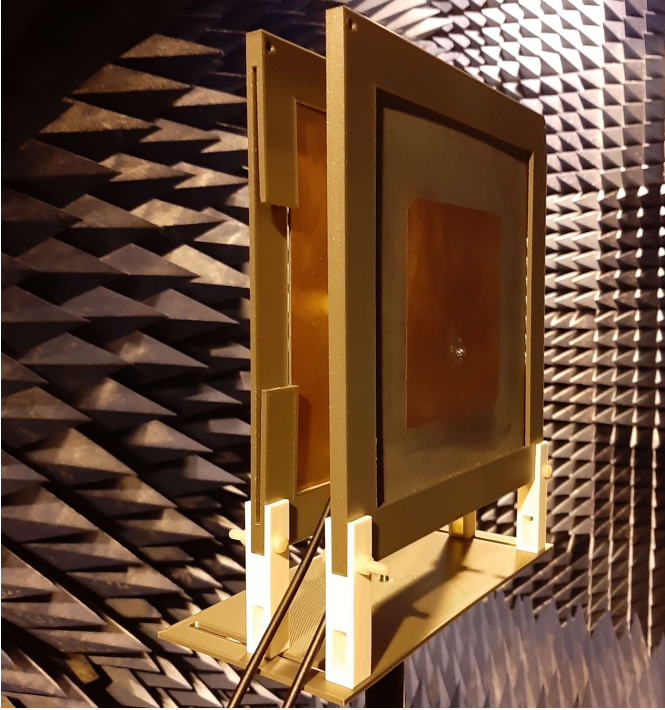


Fig. 18. Repeater configuration in the anechoic chamber.

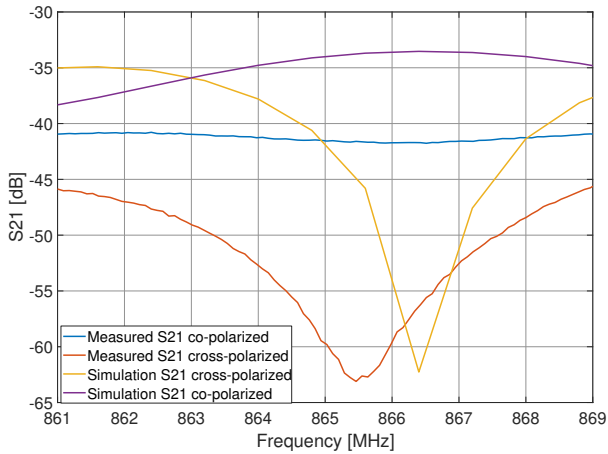


Fig. 19. S21 parameter measurements and simulation results for a repeater with two co- and cross-polarized CP antennas.

with RHCP and LHCP. The results can be seen in Fig. 19. Measurements agree well with the simulations, presented in Fig. 14. S21 measured curve actually shows a good isolation over a wider band than for the simulation. The behavior of the repeater simulated in the FDTD solver could vary slightly from reality due to the imperfect characterization of each material used in its manufacturing. Minimum coupling is measured at the desired frequency band, as expected from the theoretical analysis.

Maximum decoupling ( $\geq 60$ dB) is accomplished at 865.5 MHz. Decoupling more than 45 dB is ensured in the entire European operation band of UHF-RFID systems (865-868 MHz).

## V. REPEATER MEASUREMENTS

### A. Range Measurements with Static Repeater

In [12] the expected range improvement with the proposed repeater has been assessed and measured, using commercial equipment. Furthermore, the limitations of the structure, with respect to the expected range have been considered. In this section, we experimentally verify the expected range improvement of the proposed prototype structure. The maximum range of passive RFID tags is in the order of a few meters ( $\sim 5$ m) around the reader's antenna, depending on tag-antenna's effective aperture and the chip's sensitivity. It was shown in [12] that the repeater or a series of repeaters can arbitrarily increase the power that reaches the RFID tag and the new range depends only on the tag-to-reader link distance and the reader's sensitivity.

The power that reaches the tag at distance  $R$  from the reader antenna, by placing a repeater at distance  $x$  from the reader antenna is given by [12]:

$$P_t^{in} = \frac{P_{read}G_{read}G_t}{x^2(R-x)^2} \frac{\lambda^4}{(4\pi)^4} G_p, \quad (5)$$

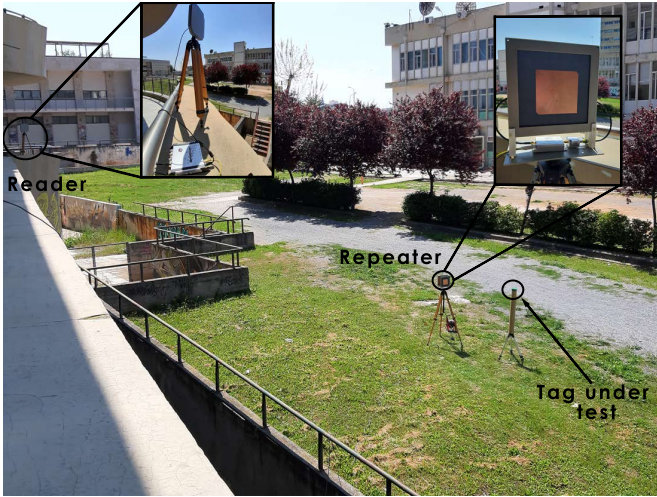
where  $P_{read}$ ,  $G_{read}$  are the reader-transmitted power and reader antenna gain towards the input antenna of the repeater,  $G_t$  is the tag's antenna gain towards the output antenna of the repeater and  $G_p$  is the expected repeater's total gain, including the two antenna gains and the amplifier.  $P_t^{in}$  should be greater than the tag's sensitivity, in order for the tag to operate. For a monostatic case, the backscattered power that reaches the reader antenna  $P_b$  is:

$$P_b = \frac{P_{read}G_{read}(\phi_r)G_t(\phi_r)G_{read}(\phi_t)G_t(\phi_{read})G_p\lambda^6}{x_1^2x_2^2R^2(4\pi)^6} M, \quad (6)$$

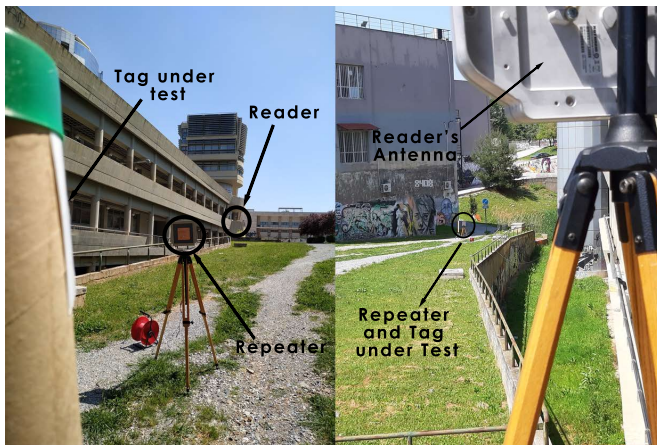
where  $\phi_r$  denotes the direction of the repeater,  $\phi_t$  the direction of the tag and  $\phi_{read}$  the direction of the reader's antenna,  $x_1$  is the reader-antenna to repeater distance,  $x_2$  is the repeater to tag distance and  $R$  is the tag to reader-antenna distance. Finally  $M$  denotes the modulation factor of the tag (typical values are around 0.1). It was shown in [12] that  $M$  depends on the incident power, due to the non-linearity of the tag-IC's front-end.

The entire structure was assembled and mounted on a tripod, as shown in Fig. 20. The structure consists of the proposed antenna-pair, a Mini-Circuits 34dB LNA amplifier [29], a Mini-Circuits 0dBm output power RF limiter (max input 1.5W) [30] and a Crystek Corporation 7MHz SAW bandpass filter, centered at 866.5MHz [31]. Three commercial passive RFID tags were selected so that each tag deploys a different RFID IC, namely 1) Alien ALN-9740 "Squiggle" with "Higgs-4" IC (-20.5dBm sensitivity), 2) Confidex "Carrier Pro" with "Impinj Monza 4QT" IC (-19.5dBm sensitivity) and 3) Tagueos "EOS-400" with "Monza R6-P" (-22.1dBm sensitivity).

Initially, the maximum range of each of the tags was measured without the repeater. The "Speedway R420" [32] monostatic RFID reader transmitted  $P_{read} = 30$ dBm from an 8.5dBic RH circularly polarized antenna, manufactured by Kathrein [33]. The transmitting antenna was placed at an elevated position from the tags to avoid the effects of the



(a) Photo of the setup at small reader-to-repeater distance (15m)



(b) View from reader and from tag for 60m-long successful passive RFID-tag identification.

Fig. 20. Measurements' Configuration.

ground reflection. The results are summarized in Table II. Then the repeater was placed at several distances and the new accomplished range after the repeater was measured; i.e. variable  $x_2$  in (6). For the expected maximum range, we have considered the reader's sensitivity  $P_b = -82.5\text{dBm}$ , instead of its nominal value ( $-85\text{dBm}$ ), due to the noise figure of the repeater (2.5dB) and solved (6) with respect to  $x_2$ . For the remaining parameters, we have considered:  $P_{read} = 30\text{dBm}$ ,  $G_{read}(\phi_r) = 8.5\text{dBic}$ ,  $G_t(\phi_r) = G_t(\phi_{read}) = 0\text{dBi}$ ,  $G_{read}(\phi_t) = 5.5\text{dBi}$  (the tag's antenna is linearly polarized).

The expected repeater's total gain  $G_p$  is calculated by adding the gain of the antenna facing the reader (6.5dBic), the gain of the antenna facing the tag (3.5dBi, since the tag is linearly polarized) and the amplifier's gain (34dB), minus the insertion losses of the three components and the connectors (1.5dB in total), hence  $G_p = 42.5\text{dB}$ .  $M$  changes with respect to the incident power at the tag's IC. Typical values of  $M$  fluctuate between 0.2 to 0.05, achieving the larger values at reduced incident power. Even though parameter  $M$  is different for each tag's IC, which would result in different expected ranges for each tag, in the results of Table II, we have assumed a constant value of  $M$  equal to 0.1 for all tags, resulting in

the same expected range. In this paper, it is not our purpose to separately characterize the performance of each tag, but rather to demonstrate the expected range improvement by deploying the proposed repeater. All tags under test were successfully identified even for a reader-repeater horizontal distance of 55m. The expected range after the repeater agrees mostly with the measurements of the Carrier Pro tag compared to the other two. Also, the achieved range after the repeater is greater at 55m for all tags with respect to the 30m reader-to-repeater distance. These deviations are due to the different  $M$  value of each tag, depolarization losses and multipath. Nevertheless, by deploying the proposed structure, we successfully identified batteryless commercial RFID tags at distances in the order of tens of meters.

### B. Mobile Repeater Measurements

Due to the small range of RFID technology, inventorying in large areas (i.e. warehouses) necessitates for the installation of a large number of RFID readers and antennas; the related cost makes this solution prohibitive. Alternatively, one could install a single reader with multiple repeaters illuminating different regions of the target area.

In this subsection, we propose placing the repeater on top of an autonomous low-cost robot. Exploiting mobility of the robot-repeater system could reduce even further the overall cost of an equivalent inventorying solution, consisting of readers and repeaters at fixed locations. A moving repeater has an additional advantage over any fixed solution: reduction of the unidentified tags due to multipath. A fixed geometry covered by fixed links may suffer from a repetitive same fading pattern. In contrast, a mobile repeater would illuminate tags from different positions diminishing fading effects.

We deployed a moving robot which can carry the repeater (see Fig. 21). We used a Turtlebot2 [34] for motion support, appropriately equipped with Lidar and a depth camera. Lidar and the camera are necessary for autonomous navigation and Simultaneous Localization and Mapping (SLAM) of the robot. These sensors are unnecessary for manual operation of the robot. The repeater was installed on top of the robot, as shown in Fig. 21.

The setup of the measurements is shown in Figs. 21- 22. Measurements were held in a rectangular type room which included 5 rows of desks with computers. 48 passive RFID tags were attached to four banners, 15 metres away from the reader antenna. 12 of the 48 tags were placed at the bottom of the banners, so that the Line-Of-Sight path from the tags to the reader's antenna is blocked by desks and computer equipment. For the reader-antenna system we used the "Speedway R420" reader by Impinj and a RH 8.5dBic circularly polarized antenna, manufactured by Kathrein. The repeater-robot starts its route from point A and reaches end point B after passing successively from each corridor.

The reader is initialized before the robot starts its route. At this point the repeater does not face the reader antenna, resulting to the identification of only 5 tags from the reader-to-tags direct link. At point A the robot starts its movement and rotates itself to pass through corridor 1. The rotation of

TABLE II  
EXPECTED AND ACHIEVED INTERROGATION RANGE OF DIFFERENT TAGS WITH AND WITHOUT THE REPEATER

Tag	Measured Range Without Repeater (m)	Repeater at 15m Expected Range after Repeater (m)	Repeater at 15m Measured Range after Repeater (m)	Repeater at 30m Expected Range after Repeater (m)	Repeater at 30m Measured Range after Repeater (m)	Repeater at 55m Expected Range after Repeater (m)	Repeater at 55m Measured Range after Repeater (m)
Carrier Pro	11	6.9	7.5	3.45	3.5	1.8	4
Squiggle	9	6.9	5	3.45	1	1.8	1.6
EOS 400	8.5	6.9	3.2	3.45	0.5	1.8	1.3

the robot enables the repeater to face both the tags and the reader-antenna, leading to a rapid increase of the number of tags identified. During the movement of the robot the number of tags identified is marked until reaching end point B. The results can be seen in Table III.

By replacing in (5) for different values of reader-to-repeater distance  $x$ , it is found that the power that reaches the tag  $P_t^{in}$  is increased when the repeater is placed closer to the tag [12]. This property is verified from the measurement-results summarized in Table III. When the robot moves along the initial corridor, 32 out of 48 tags are identified. As the robot moves along corridors which are closer to the tag, the number of identified tags increases until reaching a surprising 46/48 successfully identified tags, including 10/12 passive RFID tags under Non-Line-Of-Sight (NLOS) conditions with the reader's antenna. Successful identification of blocked tags was not expected, since the blockage along the direct tag-to-reader path was significant (multiple desks and desktop-computers). However, the motion of the robot affected the multipath contribution of components travelling from the tag to the reader. By changing the repeater's position over time, tags are illuminated from different angles, while the robot also participates in shaping the fading pattern. Thanks to the high read-rate of the reader, there are instances when multipath components contribute constructively at the receiver and NLOS passive RFID tags are identified. A representative video of the measurements is uploaded in [35].

1) *Discussion on the Mobile Repeater*: The idea of using the repeater on top of the autonomous robot (mobile-repeater) was proposed to demonstrate the properties of the repeater. We do not to claim that this represents the "best practice". In fact, placement of the fixed reader on-top of the robot (mobile-reader) would definitely outperform the mobile-repeater platform in terms of successful inventorying, since the reader-to-tag distance would be much smaller at the vicinity of the robot.

The mobile-repeater would outperform the mobile-reader in terms of cost, only under the assumption that multiple low-cost robots are deployed concurrently in different regions of a larger area. Considering that the robotic platform with its sensors and the repeater would cost around 1000\$, the fixed reader with its antennas costs approximately 2000\$, then the mobile-reader would cost 3000\$. By deploying  $n$  mobile-repeaters with a single fixed reader, the cost would be  $2000\$ + k1000\$$ , while the corresponding cost with multiple robots would be  $k3000\$$ ; for increasing  $k$ , the difference becomes significant.

TABLE III  
NUMBER OF INTERROGATED TAGS VS TRACE OF ROBOT

	Starting Point	After Corridor 1	After Corridor 2	After Corridor 3	After Corridor 4
Tags Identified	5	32	43	45	46

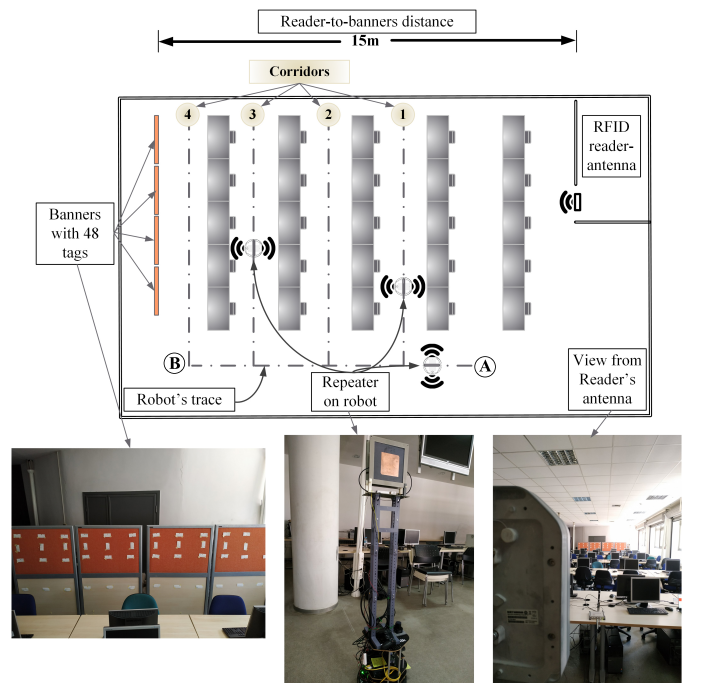


Fig. 21. Measurements' setup, Top view

We intend to use the repeater in a fixed installation inside a large exhibition area, to track the location of the visitors and create statistics on their interactions with the exhibits. Each visitor holds an RFID-tagged ticket. Thanks to the repeater, we can successfully track the location of the visitor in the entire exhibition area; which would not be possible with a single-reader installation. The motion of the visitor is expected to have similar effects to what was experienced previously due to the motion of the robot; thanks to the mobility and its effects on changing multipath, the visitor is expected to be identified even at greater distances.

## VI. CONCLUSION

In this paper, we designed and constructed a prototype UHF forward-link repeater. We focused on the design of



Fig. 22. Measurements' setup, view from reader-antenna

the antenna-pair, such that sufficient decoupling is ensured between the two antennas which operate at great vicinity, while keeping the volume of the structure small. The input RF-signal in the first antenna is filtered and amplified, before being re-transmitted by the second antenna. Decoupling from the second to the first antenna should exceed the amplification of the structure, typically above 40dB. We proposed the design of circularly polarized microstrip antennas with inverse polarization handedness. The proposed structure *i*) fully exploits the circularly polarized incident field from the RFID-reader antenna, maximizing the gain, *ii*) retransmits a circularly polarized field towards the tags, improving the probability of successful reception of the incident field at the randomly oriented tag's antenna and *iii*) maintains a small volume, while adhering to the strict decoupling constraint. A decoupling of more than 65dB has been predicted and measured in the entire European operation band of UHF-RFID systems.

The prototype structure was constructed and measured outdoors. Commercial passive RFID tags were successfully interrogated at 59m from a monostatic UHF RFID reader, by placing the repeater at a distance of 55m from the reader. To the best of our knowledge, this is the first time that such a structure is constructed and measured. The experimental results agreed well with the theoretical expectations. Furthermore, we placed the repeater on top of a low-cost autonomous robot. Thanks to the mobility of the robot, passive RFID tags were identified even at NLOS locations. This property can also be exploited inversely; i.e. placement of a fixed repeater to track moving tags at great distance represents a low-cost alternative to placement of multiple readers.

## REFERENCES

- [1] G. A. Vera, Y. Duroc, S. Tedjini, "Analysis of Harmonics in UHF RFID Signals," *IEEE Trans. Microwave Theory and Techniques*, vol. 61, no. 6, pp. 2481-2490, June 2013.
- [2] G. A. Vera, S. D. Nawale, Y. Duroc, S. Tedjini, "Read Range Enhancement by Harmonic Energy Harvesting in Passive UHF RFID," *IEEE Microwave and Wireless Components Letters*, vol. 25, no. 9, pp. 627-629, Sept. 2015.
- [3] S. Chen, S. Zhong, S. Yang, X. Wang, "A Multiantenna RFID Reader With Blind Adaptive Beamforming," *IEEE Internet of Things Journal*, vol. 3, no. 6, pp. 986-996, December 2016.
- [4] M. S. Trotter, J. D. Griffin, G. D. Durgin, "Power-Optimized Waveforms for Improving the Range and Reliability of RFID Systems," *2009 IEEE International Conference on RFID*, pp. 80-87, Orlando, Florida, USA, April 2009.
- [5] A. Boaventura, D. Belo, R. Fernandes, A. Collado, A. Georgiadis, N. B. Carvalho, "Boosting the Efficiency: Unconventional Waveform Design for Efficient Wireless Power Transfer," *IEEE Microwave Magazine*, vol. 16, no. 3, pp. 87-96, April 2015.
- [6] J. Kimionis, A. Bletsas, J. N. Sahalos, "Increased range bistatic scatter radio," *IEEE Trans. Commun.*, vol. 62, no. 3, pp. 1091-1104, Mar. 2014.
- [7] P. N. Alevizos, K. Tountas, A. Bletsas, "Multistatic scatter radio sensor networks for extended coverage," *IEEE Trans. Wireless Commun.*, vol. 17, no. 7, pp. 4522-4535, Jul. 2018.
- [8] Mojix Star System, [Online]. Available: <https://mojix.com/starflex-enterprise-class-rfid-reader/>. [Accessed: 21- Sep.- 2020].
- [9] R. Sadr et al., *RFID systems using distributed exciter network*, Mar. 2014, US Patent 8,680,970 B2. [Online]. Available: <https://patents.google.com/patent/US8680970>. [Accessed: 21- Sep.- 2020].
- [10] Z. Fu, M. J. Crisp, S. Yang, R. V. Penty, I. H. White, "Long distance passive UHF RFID system over ethernet cable," in *Proc. IEEE RFID Techn. and Applications (RFID-TA)*, Warsaw, Poland, Sep. 2017, pp. 294-298.
- [11] A. P. Sample, J. Braun, A. Parks, J. R. Smith, "Photovoltaic enhanced UHF RFID tag antennas for dual purpose energy harvesting," in *2011 IEEE International Conference on RFID*, Orlando, Florida, April 2011.
- [12] A. G. Dimitriou, "Design, Analysis and Performance Evaluation of a UHF RFID Forward-Link Repeater," *IEEE Journal of Radio Frequency Identification*, EARLY ACCESS.
- [13] J. D. Park, M. Rahman, H. N. Chen, "Isolation Enhancement of Wide-Band MIMO Array Antennas Utilizing Resistive Loading," *IEEE Access*, Vol. 7, 2019.
- [14] A. C. K. Mak, C. R. Rowell, R. D. Murch, "Isolation Enhancement Between Two Closely Packed Antennas," *IEEE Transactions on Antennas and Propagation*, Vol. 56, No. 11, 2008.
- [15] S. Zhang, Z. Ying, J. Xiong, S. He, "Ultrawideband MIMO/Diversity Antennas With a Tree-Like Structure to Enhance Wideband Isolation," *IEEE Antennas and Wireless Propagation Letters*, Vol. 8, 2009.
- [16] S. C. Chen, Y. S. Wang, S. J. Chung, "A Decoupling Technique for Increasing the Port Isolation Between Two Strongly Coupled Antennas," *IEEE Transactions on Antennas and Propagation*, Vol. 56, No. 12, 2008.
- [17] L. Zhao, L. K. Yeung, K. LiWu, "A Coupled Resonator Decoupling Network for Two-Element Compact Antenna Arrays in Mobile Terminals," *IEEE Transactions on Antennas and Propagation*, Vol. 62, No. 5, 2014.
- [18] C. M. Luo, J. S. Hong, L. L. Zhong, "Isolation Enhancement of a Very Compact UWB-MIMO Slot Antenna With Two Defected Ground Structures," *IEEE Antennas and Wireless Propagation Letters*, Vol. 14, 2015.
- [19] Y. Chung, S. S. Jeon, D. Ahn, J. I. Choi, T. Itoh, "High Isolation Dual-Polarized Patch Antenna Using Integrated Defected Ground Structure," *IEEE Microwave and Wireless Components Letters*, Vol. 14, No. 1, 2004.
- [20] M. A. U. Haq, S. Koziel, "Ground Plane Alterations for Design of High-Isolation Compact Wideband MIMO Antenna," *IEEE Access*, Vol. 6, 2018.
- [21] K. Buell, H. Mosallaei, K. Sarabandi, "Metamaterial Insulator Enabled Superdirective Array," *IEEE Transactions on Antennas and Propagation*, Vol. 55, 2007.
- [22] G. Zhai, Z. N. Chen, X. Qing, "Enhanced Isolation of a Closely Spaced Four-Element MIMO Antenna System Using Metamaterial Mushroom," *IEEE Transactions on Antennas and Propagation*, Vol. 63, 2015.
- [23] M. A. Abdalla, A. A. Ibrahim, "Compact and Closely Spaced Metamaterial MIMO Antenna With High Isolation for Wireless Applications," *IEEE Antennas and Wireless Propagation Letters*, Vol. 12, 2013.
- [24] K. Komaki, H. Iwasaki, "Back to Back Patch Antenna Operated Orthogonal Polarization for Repeater Use," *IEEE 2015 International Symposium on Antennas and Propagation (ISAP)*, 2015.
- [25] J. R. James, P. S. Hall, "Handbook of Microstrip Antennas," IEE Electromagnetic Waves Series, 1989.
- [26] C. A. Balanis, "Antenna Theory: Analysis and Design, Fourth Edition," Wiley, 2016.
- [27] M. Haneishi, S. Yoshida, "A design method of circularly polarized rectangular microstrip antenna by one-point feed," *Electronics and Communications in Japan*, Vol. 64-B, No. 4, 1981.
- [28] S. M. Palhade, S. P. yawale, "Design and photo-lithographic fabrication of microstrip patch antenna," *International Journal of Science and Research*, Vol. 4, 2015.
- [29] ZRL-1150LN+ 34dB Low Noise Amplifier - Mini Circuits, [Online]. Available: <https://www.minicircuits.com/pdfs/ZRL-1150LN+.pdf>. [Accessed: 21- Sep.- 2020].

- [30] ZFLM-252-1WL-S+ 0dB RF Limiter - Mini Circuits, [Online]. Available: <https://www.minicircuits.com/pdfs/ZFLM-252-1WL-S+.pdf>. [Accessed: 21- Sep.- 2020].
- [31] CBPFS-0866 7MHz Saw Band Pass Filter - Crystek Corporation, [Online]. Available: <https://www.crystek.com/microwave/specsheets/filter/CBPFS-0866.pdf>. [Accessed: 21- Sep.- 2020].
- [32] Speedway R420 RFID Reader - Impinj, [Online]. Available: <https://www.impinj.com/platform/connectivity/speedway-r420/>. [Accessed: 21- Sep.- 2020].
- [33] Kathrein RFID Antennas, [Online]. Available: <https://www.kathrein.com/en/solutions/internet-of-things-neu/products/hardware/wide-range-70-antennas/#c813>. [Accessed: 21- Sep.- 2020].
- [34] Turtlebot 2 Platform, [Online]. Available: <http://www.turtlebot.com/turtlebot2/> [Accessed: 21- Sep.- 2020].
- [35] Video of the Repeater on Top of a Robot, [Online]. Available: <https://youtu.be/U7DZJKOYX7g> [Accessed: 21- Sep.- 2020].



**Spyros Megalou** received the MSc degree in Electrical and Computer engineering from the Aristotle University of Thessaloniki, Greece, in 2019, and he is currently pursuing the PhD degree at the same School. His main research interests include RFID technology, localization techniques, microwave applications and antenna design. He is also a member of a space related group (BEAM, Beyond Earth Aristotle Missions) focusing on space experiments and applications.



**Antonis G. Dimitriou** (S'01-M06-SM'14) received the diploma and the Ph.D degree in Electrical and Computer Engineering from the Aristotle University of Thessaloniki, Greece, in 2001, and 2006 respectively. Since 2007, he is with the School of Electrical and Computer Engineering of AUTH, where he currently serves as a teaching and research faculty member.

He has participated in more than 20 research projects, 8 of which since 2007 as a principal investigator in the fields of Robotics, RFIDs, and Wireless Sensor Networks. He is currently the coordinator of project "RELIEF", involving continuous RFID inventorying through robotics and project "CULTUREID", where prototype repeaters will be installed inside large exhibition areas to monitor RFID tagged exhibits and visitors. He was a Management Committee Member in the ICT COST Action IC301 "Wireless Power Transmission for Sustainable Electronics (WiPE)". He is the author or co-author of approximately 60 journal and conference papers.

Dr. Dimitriou was the recipient of the Ericsson Award of Excellence in Telecommunications in 2001 and co-recipient of the student-paper award in the 2011 IEEE RFID-TA conference. He received the "IEEE Wireless Communications Letters Exemplary Reviewer" award in 2012 and 2014. He is a Senior IEEE Member since February 2014. He also serves as a reviewer for major journals and as a TPC member for international conferences.



**Anastasios Tzitzis** was born in Thessaloniki, Greece, in 1994. In 2018 he received the Diploma in Electrical and Computer Engineering from Aristotle University of Thessaloniki, where he is currently working toward the Ph.D. degree. At the same time, he is working as a Research and Teaching Assistant at the Aristotle University. His current research interests include analysis and design of antennas, RFID technology and wave propagation.



**Traianos V. Yioultsis** (M'09) received the Diploma and the Ph.D. degrees in electrical and computer engineering from the Aristotle University of Thessaloniki, Greece, in 1992 and 1998, respectively. From 2001 to 2002, he was a Post-Doctoral Research Associate with the Department of Electrical and Computer Engineering, University of Illinois at Urbana-Champaign. Since 2002, he has been with the Department of Electrical and Computer Engineering, Aristotle University of Thessaloniki, where he is currently a Professor. His current interests include the analysis and design of antennas and microwave circuits with fast computational techniques, and the modeling of complex wave propagation problems. He has also served as a member of the Editorial Board for IEEE Communications Letters and several international conferences.